JKAU: Earth Sci., **Vol. 21**, No. 1, pp: 137-169 (2010 A.D. / 1431 A.H.)
DOI: 10.4197 / Ear. 21-1.6

Mineral Chemistry and Genesis of Uranyl Minerals Associated with Psammitic Gneisses, Abu Rusheid Area, South Eastern Desert of Egypt

Yehia H. Dawood
Fac. of Earth Sciences, King Abdulaziz University, Jeddah, Saudi Arabia
yhdawood@yhaoo.com

Received: 14/2/2009 Accepted: 25/12/2009

Abstract. Meta-autunite, uranophane, boltwoodite and soddyite are found as yellow crusts and acicular crystals in the voids, fractures and shear zones in the psammitic gneisses of Abu Rusheid area. Optical microscopy, X-Ray Diffraction (XRD), Backscattered Electron (BSE) and Secondary Electron (SE) Imaging, Energy Dispersive X-Ray Spectrometry (EDS) and quantitative Electron Probe Micro Analyses (EPMA) have been used to determine the mineralogical composition, behavior and fate of major and trace elements in the gneissic weathering profile. Coupled substitutions in meta-autunite, Na proxy for K in boltwoodite and formation of soddyite at the expense of uranophane are evident in the study area. Apparently the effect of metamorphism on the pre-existing uranium was limited to a more or less in situ remobilization and concentration. The uranyl minerals appear to be derived from the host rock after being exposed to a long period of alteration and rock–fluids interaction. The segregation of uranyl minerals was driven by the compositional contrast between the migrating fluids and in situ wall rock composition of the fractures. The composition and genesis of uranyl mineralization associated with Abu Rusheid gneisses provide additional information about the behavior of radionuclides in arid environments and at very oxidizing conditions.

Keywords: Mineral chemistry; Meta-autunite; Uranyl silicates; Abu Rusheid; Eastern Desert; Egypt.

Introduction

Uranium minerals can be classified into two categories: reduced species that contain most of uranium as U^{4+} and oxidized species or uranyl minerals that contain uranium as U^{6+}. The 6+ oxidation state is the most stable and forms soluble uranyl complex ion UO_2^{2+} that plays a crucial role in uranium mobility. Uranium minerals have been a subject of an increased attention due to the interest in uranium as an energy resource, and more recently, in its role in environmental problems associated with the disposal of radioactive waste and the remediation of contaminated sites. Natural environments provide helpful information on movement and retardation mechanisms of radionuclides in nature and could be used to create and test models of the long-term behavior of spent nuclear fuel in the lithosphere. The radionuclides released during the corrosion of primary uranium minerals may become incorporated into the structures of the secondary uranyl phases (Ewing, 1991 and 1993). Therefore, investigations of primary uranium minerals and migration of their components during corrosion as well as genesis of uranyl phases have been extensively examined in the last few years (Janeczek *et al.*, 1996; Fayek *et al.*, 1997; Fayek *et al.*, 2002; Jerden and Sinha, 2006 and Gorman-Lewis *et al.*, 2007). Recently, the role of the thermodynamic database of uranyl minerals for understanding the mobility of uranium in the environment was demonstrated by Gorman-Lewis *et al.* (2008).

Uranyl minerals have been reported from different localities in the Eastern Desert of Egypt. They are mostly associated with granitic and alkaline volcanic rocks. El Erediya and Gattar plutons are examples for the granitic rocks hosting uranium deposits whereas El Atshan alkaline trachyte represents the most pronounced uranium occurrence associated with volcanic rocks. Different varieties of uranyl minerals have been reported from these rocks including uranophane, soddyite, kasolite, meta-autunite and zippeite.

Abu Rusheid area is a distinctive occurrence of uranyl mineralization in Egypt where the host rocks are represented by gneisses. This paper summarizes electron microprobe data of uranyl mineral phases from Abu Rusheid area. This gives insight into the chemistry of fluids responsible for the formation of these minerals and a better understanding of the mineral genesis controls. This also may assist in the recognition of the radionuclides behavior in such host rock and in an arid environment.

Geologic Setting and Petrography

Abu Rusheid area lies to the SE of the Migif-Hafafit metamorphic core complex. This complex represents one of three major domal structures in the Eastern Desert of Egypt: Gabal Meatiq (Loizenbauer *et al.*, 2001), Abu Swayel (Abd El-Naby and Frisch, 2002), and Migif-Hafafit area (Fowler and El Kalioubi, 2002 and Abd El-Naby *et al.*, 2008). The geology of Hafafit area has been documented as a highly complex and many hypotheses have been proposed for the tectonic evolution of this area (Fowler and Osman, 2009). The rock assemblages at Hafafit area could be grouped into two main units which are separated by Nugrus Thrust (Abd El-Naby and Frisch, 2006). The western unit (Hafafit unit) consists of Hafafit domes which include from core to rim granite gneiss of tonalitic and trondhjemitic composition, banded amphibolite which is overthrusted by ultramafic rocks, alternating bands of biotite- and hornblende-gneiss and the psammitic gneisses at the rim of the domal structure. The eastern unit (Nugrus unit) is composed mainly of low grade mica-schists and metavolcanics. Both units have been intruded by undeformed leucogranites, especially along thrust zones.

Pan African Rock Units at Abu Rusheid Area

Abu Rusheid area is located between a major thrust to the NE and a minor one to the SW (Fig. 1a). The main rock units encountered in this area are metasediments, ophiolitic mélange, amphibolites, metagabbros, hornblende gneisses, psammitic gneisses and leuco- and pink granites. The metasediments are represented mainly by separated successions of highly foliated mica schist locally thrusted over the psammitic gneisses (Fig. 1 a and b). Tourmaline mineralization occurs in different parts of the metasediments either as disseminated crystal clusters or as discontinuous tourmalinite bands (Harraz and El-Sharkawy, 2001). The ophiolitic mélange represents the hanging wall of the major thrust in the study area (Fig. 1a). It comprises a metamorphosed sedimentary matrix enclosing amphibolite sheets, allochthonous serpentinite and gabbroic masses, as well as quartzitic bands. Amphibolites and metagabbros are probably related to the calc-alkaline metagabbros associated with Hafafit gneisses (El Ramly *et al.*, 1993). The hornblende gneisses are coarse to medium grained and highly foliated.

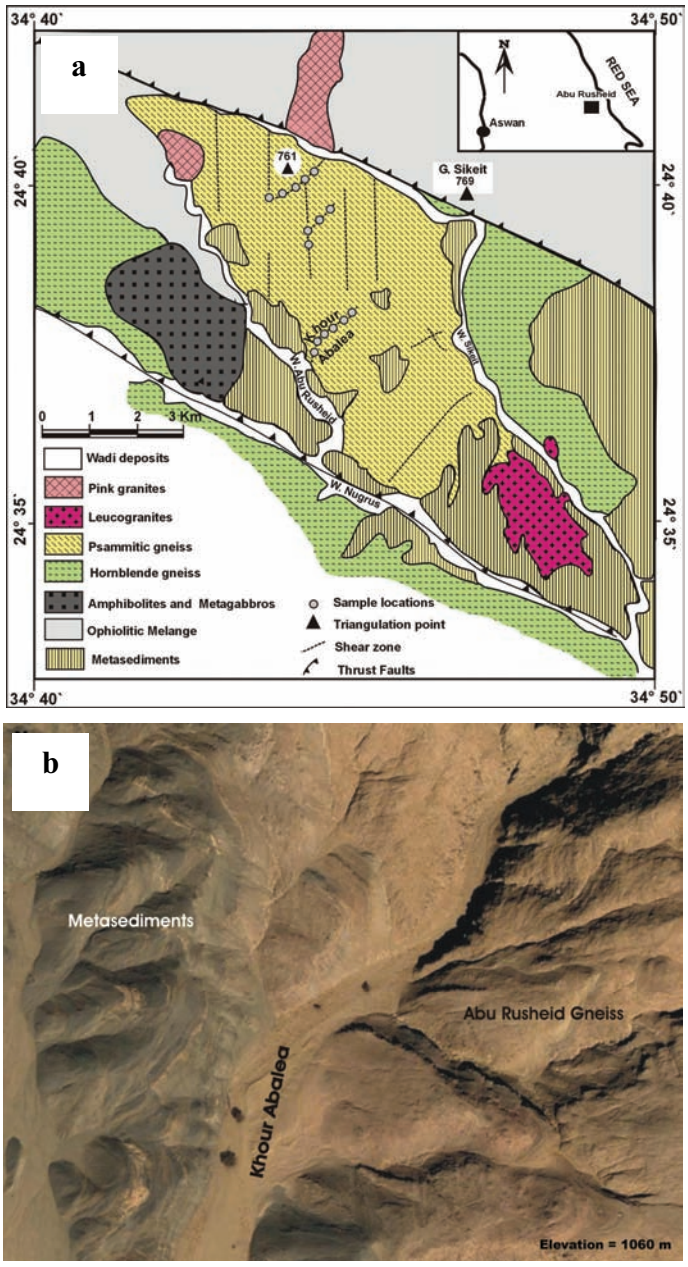

Fig. 1. a. Geologic map of the study area showing sample locations (modified after Greiling *et al.*, 1988). b. Satellite image showing part of Khour Abalea and the metasediments thrust over Abu Rusheid gneisses.

Although Abu Rusheid gneisses were originally identified as psammitic gneisses (Hassan, 1973; Abdel Monem and Hurley, 1979; Hilmy *et al.*, 1990; Abd El-Naby and Frisch, 2006), some authors described these rocks as gneissic granites (Ibrahim *et al.*, 2000; Raslan, 2008) and cataclastic granites (Ibrahim *et al.*, 2007). In the present study, these rocks are classified as psammitic gneisses due to: 1) Its relatively lower relief compared to granitic rocks, 2) Their high silica contents (more than 80% SiO_2, in average, Abd El-Naby and Frisch, 2006), 3) Their high contents of quartz grains, mostly of equal sizes (Fig. 2 a-c), 4) Separated zircon grains from the rocks gave U/Pb age of 1770 Ma that interpreted as a probable age of the crustal area that supplied the detritus forming the original sediments (Abdel-Monem and Hurley, 1979). Furthermore, the geochemical data of these gneisses suggest sedimentary protolithes ranging from lithic arenite to arkose (Abd El-Naby and Frisch, 2006). The depositional environment of this sedimentary protolithes was in an active continental margin setting (Roser and Korsch, 1986).

Abu Rusheid gneisses are highly mylonitized and dissected by several shear zones mostly oriented to north and north east directions (Fig. 1a). Brecciation resulting from faulting reactivation is found in some parts along the shear zones. The psammitic gneisses show a well developed planer banding, gneissosity and folding. Lineation, defined by mineral streaking is well marked on the foliation surfaces (Hassan, 1973). Small size quartz and pegmatitic veins are common and seem to be developed from the gneiss through mobilization and crystallization as they fade out into the gneiss with no sharp contacts (Hassan, 1973). These pegmatite veins are abundant along Khour Abalea shear zone.

Petrographically, Abu Rusheid gneisses are composed mainly of quartz, in addition to feldspars, biotite and muscovite with minor zircon, garnet, sulphides, apatite, monazite, uranium-rich thorite and magnetite. Furthermore, ishikawaite, uranium-rich samarskite [U, Fe, Y, Ca) (Nb, Ta)O_4] was reported by Raslan (2008) in these rocks. Quartz constitutes more than two thirds of the rock. The quartz grains are colourless rounded to subrounded, locally showing granoblastic texture with well developed sutures among equal sized-grains (Fig. 2 a-c). Also, it occurs as inclusions in other minerals and as infiltration and replacement along the cleavage of mica flakes. Feldspars are represented mainly by

colourless subhedral crystals of potash feldspars and subhedral to euhedral prismatic crystals of plagioclase. The K-feldspars are partially altered to kaolinite whereas the plagioclase crystals are occasionally sericitised. Biotite flakes are pale brown to yellowish brown and show iron oxides inclusions. Some of these flakes show alteration to chlorite. Garnet occurs as colorless subhedral to anhedral grains with quartz inclusions. Sulphide minerals, represent-ed mainly by pyrite, are scattered in the studied gneisses (Fig. 2a) (Mansour, 2005). Zircon is found as pale yellow to pale brown euhedral prismatic crystals with bipyramidal terminations. Opaque mineral inclusions of different sizes and types are present in the mineral (Fig. 2b). Metamict zircon grains are common and zoned varieties are occasionally present reflecting an over-growth during metasomatism (Hassan, 1973).

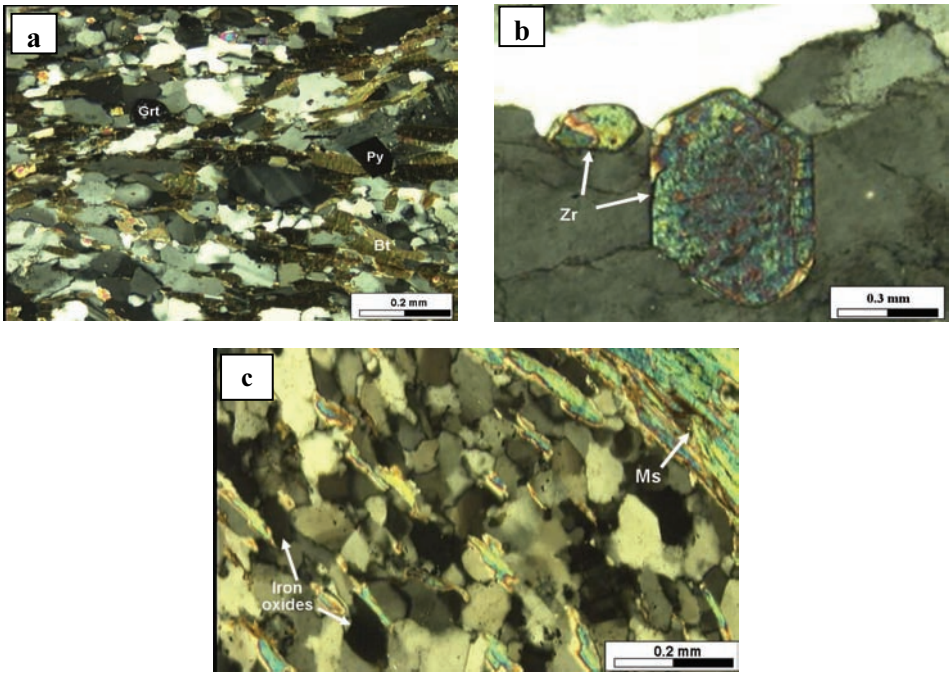

Fig. 2. Photomicrographs of the psammitic gneisses showing: a) Rounded to subrounded quartz grains, anhedral garnet grain (Grt), biotite flakes (Bt) and dodecahedron crystal of pyrite (Py), (C.N.), b) Two prismatic zircon grains (Zr) with bipyramidal terminations intergrown with plagioclase and quartz. The mineral shows opaque inclusions, Metamict-ization and zoning, (C.N), c) Subrounded quartz grains, iron oxides and muscovite flakes (Ms) as essential constituents of Abu Rusheid gneisses.

The latest Pan-African activity in the mapped area is represented by a suite of leucogranites, pink granites and minor intrusions of felsite and aplite. The younger granites are locally developed along thrust faults and contain numerous enclaves from older rocks particularly mica schist. Several masses of these granites are found in Wadi Nugrus-Abu Rusheid. They form small lens-like plutonic masses (Fig. 1a). Generally, the leucogranites are medium- to course-grained, composed mainly of quartz, K-feldspar, plagioclase, garnet, biotite and muscovite. On the other hand, the pink granites are more enriched in K-feldspars and quartz. The emplacement of leucogranites (594-610 Ma) is related to the late Neoproterozoic extension following continental collision (Moghazi *et al.*, 2004). The latest phase of magmatic activity is represented by minor emplacements of felsite and aplite which intruded the Hafafit gneisses and the ophiolitic assemblage (El-Ramly *et al.*, 1993).

Surficial Processes and Formation of Secondary Minerals

The effects of the hydrothermal solutions on the Abu Rusheid gneisses were reported by El Shazly and Hassan (1972), Hassan (1973), Abdel-Monem and Hurley (1979) and Ibrahim *et al.* (2000). The gneisses exhibit extensive alteration, including silicification, sericitization, kaolinitization, chloritization, hematitization and limonitization (Abd El-Naby *et al.*, 2008). These alterations are closely associated with the shear zones indicating that some of these fractures have worked as channel-ways for metasomatizing fluids. Alunite $[KAl_3(SO_4)_2(OH)_6]$ is found as white color massive materials filling some parts of the shear zones, particularly those which have been subjected to severe alteration. The existence of alunite may be brought about by oxidation of sulphides and formation of sulphuric acid. The acid, in turn, reacted with the orthoclase feldspar-rich parts of the rocks to form alunite (Dill, 2001 and Lerouge *et al.*, 2006). Hassan (1973) classified the gneisses into four divisions depending upon mineral composition and intense of metasomatic effects. The uppermost division of the gneisses was refereed as amazonite-bearing psammitic gneiss which is highly metasomatized and reflects high radioactive anomalies. Uranophane was reported from this division by Abd El-Naby and Frisch (2006). Autunite, meta-autunite, kasolite and torbernite were also reported by Ibrahim *et al.*, (2007). This division of the gneisses contains abundant crystals of zircon, fluorite and

columbite. Fluorite occurs in the form of anhedral grains moulded around quartz and feldspar crystals indicative of the great mobility of fluorine during metasomatic processes (Hassan, 1973). Columbite $(Fe,Mn)Nb_2O_6$ occurs in minute crystals (0.1-0.5 mm) dispersed in the gneisses particularly in the parts that were affected by metasomatism. It attains large sizes (up to 1 cm) in the pegmatitic veins (Sabet *et al.*, 1976).

The occurrence of the different mineral varieties in the psammitic gneiss is largely due to the variation in the mineralogical composition of the sedimentary protolithes and the effects of alteration and supergene processes. Some of these minerals are inherited from the pre-metamorphic rocks such as zircon and some are introduced to the rock by hydrothermal activity such as fluorite and alunite and others have been formed by supergene enrichment such as uranophane.

Methods of Study

Fifteen samples were collected from the mineralized zones of Abu Rusheid gneisses (Fig. 1a). The collected samples show variable degrees of alteration and surficial aggregates of yellow colored uranyl mineralization. Some other fresh samples were collected to study the petrographic characteristics of the host rock. Crusts of uranyl minerals have been scraped from the surfaces of these samples using a blade. Some of the scraped minerals were isolated under binocular microscope based on their color and identified using X-Ray Diffraction technique. Siemens powder X-ray diffractometer was used with D 500 goniometer and a graphite monochrometer. The pulverized samples were scanned at a rate 1 degree 2θ per half minute with step size 0.02 2θ. Moreover, crusts of the scraped uranyl mineralization were mounted with epoxy on glass slides then ground to the desired thickness prior to polishing. Mineralogical characteristics and chemical compositions of uranyl minerals were determined by a fully automated JEOL JXA-8900 Electron Probe Micro Analyzer available at the Institut für Geowissenschaften - Mineralogie und Geodynamik- der Universität Tübingen, Germany. Back Scattered Electron (BSE) and Secondary Electron (SE) imaging were used to illustrate the textural and mineralogical characteristics of the samples. Energy Dispersive X-Ray Spectrum (EDS) was used to qualitatively measure the elemental composition. The operating voltage is 15 kV, the beam diameter is 2μm and the counting time is 30s per

element. Sixty analyses were performed on twenty mineral grains using natural and synthetic standards. Setup and operating conditions for uranyl minerals EPM analyses are presented in Table 1. Data reduction for the various elements was performed by taking into account the matrix corrections between standards and samples and the analytical parameters. The matrix effects were corrected by the conventional ZAF method. Moreover, special care was taken to ensure that line overlaps were properly corrected. Errors in microprobe analyses due to counting statistics are generally less than 1% in most of the analyzed elements.

Table 1. Setup and operating conditions for uranyl minerals EPM analyses.

Elem.	Line	Std.	Crystal	Bkg high (+)	Bkg low (-)	Baseline (V)	Window (V)	Bias (V)	Detection limit (ppm)
Si	Kα1	wallastonite	PETH	5.00	5.00	0.70	9.30	1722	103
P	Kα1	$CePO_4$	TAP	5.00	4.96	0.70	9.30	1700	235
U	Mα1	UO_2	PETH	5.00	5.00	0.70	9.30	1722	241
Ca	Kα1	wallastonite	PETJ	5.00	5.00	0.70	9.30	1686	133
Al	Kα1	Al_2O_3	TAP	5.00	5.00	0.70	9.30	1688	50
V	Kα1	V_2O_3	PETJ	5.00	5.00	0.70	9.30	1700	80
K	Kα1	K-feldspar	TAP	5.00	5.00	0.70	9.30	1700	180
Na	Kα1	Albite	TAP	5.00	5.00	0.70	9.30	1700	110
Mg	Kα1	MgO	TAP	5.00	5.00	0.70	9.30	1688	110
Pb	Mα1	PbVGe Oxides	PETH	5.00	5.00	0.70	9.30	1722	70
Fe	Kα1	Fe_2O_3	LIFH	5.00	5.00	0.70	9.30	1700	60
As	Lα1	As_2O_5	TAP	5.00	5.00	0.70	9.30	1688	140
La	Lα1	$LaPO_4$	LIF	5.00	5.00	0.70	9.30	1720	350
Ce	Lα1	$CePO_4$	PETJ	5.00	5.00	0.70	9.30	1714	90
Pr	Lα1	$PrPO_4$	LIFH	5.00	5.00	0.70	9.30	1714	80
Nd	Lα1	$NdPO_4$	LIF	5.00	5.00	0.70	9.30	1720	230
Sm	Lα1	$SmPO_4$	LIFH	5.00	5.00	0.70	9.30	1722	50
Eu	Lα1	$EuPO_4$	LIFH	5.00	5.00	0.70	9.30	1722	50
Gd	Lα1	$GdPO_4$	LIF	5.00	5.00	0.70	9.30	1720	378
Tb	Lα1	$TbPO_4$	LIFH	5.00	5.00	0.70	9.30	1722	60
Dy	Lα1	$DyPO_4$	LIFH	5.00	5.00	0.70	9.30	1722	100
Ho	Lα1	$HoPO_4$	LIFH	5.00	5.00	0.70	9.30	1722	440
Er	Lα1	$ErPO_4$	LIFH	5.00	5.00	0.70	9.30	1722	50
Tm	Lα1	$TmPO_4$	LIFH	5.00	5.00	0.70	9.30	1722	50
Yb	Lα1	$YbPO_4$	LIFH	5.00	5.00	0.70	9.30	1722	60
Lu	Lα1	$LuPO_4$	LIFH	5.00	5.00	0.70	9.30	1722	100

Results

The yellow color uranyl mineralization is found in the uppermost part of the Abu Rusheid gneisses along the shear zones, faults and fractures, particularly those trending NE and at their intersections. The Khour Abalea shear zone has one of the most pronounced uranyl mineralization in the study area. This shear zone cuts the gneisses from its central part in nearly NE direction (Fig. 1). The uranyl mineralization is mainly associated with hematitization and argillic alterations (Fig. 3). XRD investigation of the scraped uranyl mineral crusts showed the patterns of meta-autunite, uranophane, soddyite and boltwoodite. These mineral phases are also identified using EDS, BSE and SE images as well as quantitative EPMA.

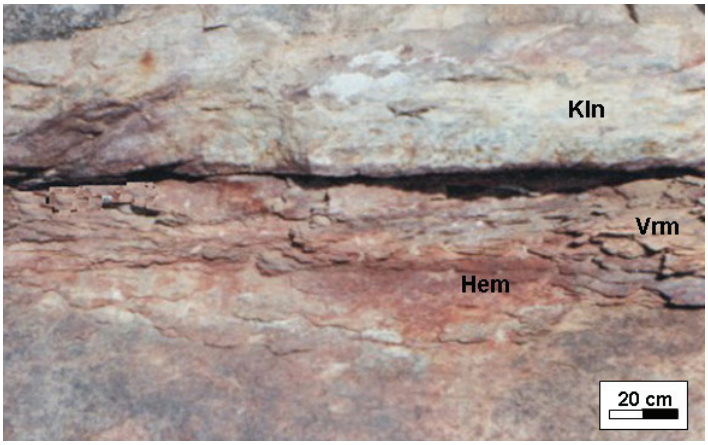

Fig. 3. Photograph shows iron oxides (mainly hematite, Hem) and flakey vermiculite (Vrm) filling a joint in the gneisses. Also shows white colored argillic alteration (mainly kaolinite, Kln) of the country rocks.

Uranyl Phosphates

Meta-autunite [$Ca(UO_2)_2(PO_4)_2$:2-6H_2O] represents the main uranyl phosphate mineral in the study area (Fig. 4a and b). The aggregates of meta-autunite are soft and consist of lemon yellow to greenish yellow small crystallites with a micaceous habit (Fig. 4a). Occasionally meta-autunite is found as tabular square crystals often in parallel growths and terminated by bipyramidal forms (Fig. 4a). The largest crystal attains maximum length of 83 μm and width of 35 μm. The cracking is likely caused by a volume change brought about by dehydration process. The thin crystals or cleavage sheets of meta-

autunite are bendable. Table 2 shows representative EPM analyses of meta-autunite. UO_3 ranges from 63.95 to 80.78 with an average of 71.10%, P_2O_5 ranges from 8.97 to 10.95 with an average of 9.70%, CaO ranges from 1.15 to 1.91 with an average of 1.59%.

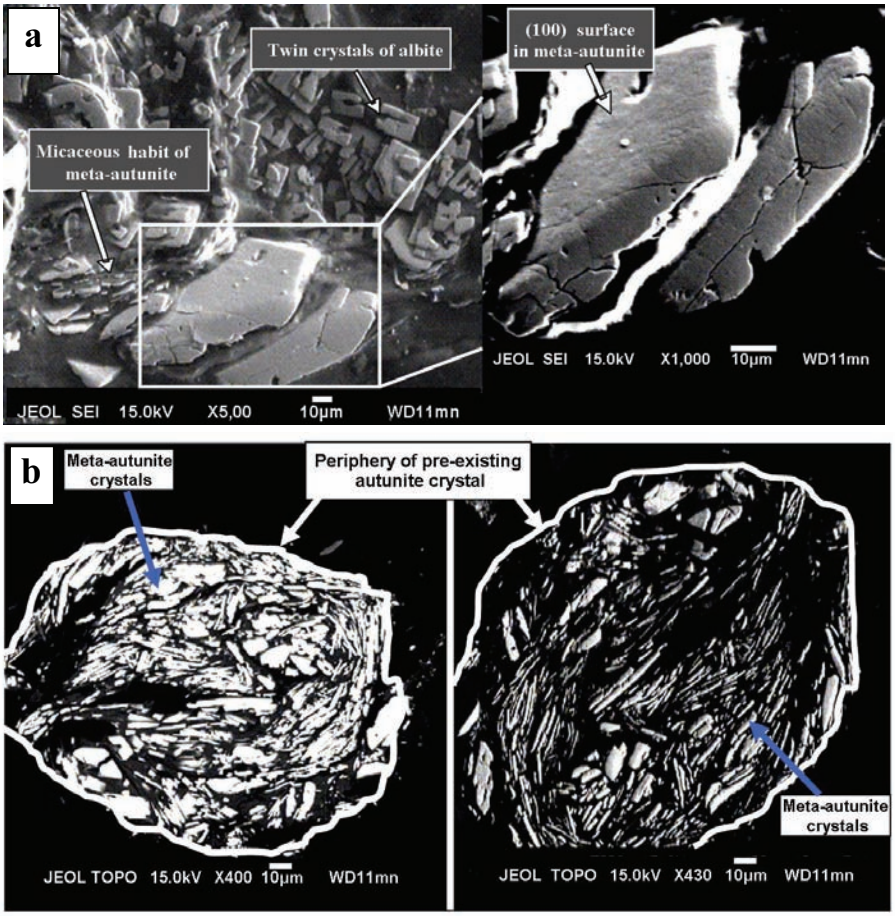

Fig. 4. a) Secondary Electron Images (SEI) showing two euhedral meta-autunite crystals and micaceous aggregates of the same mineral associated with twin crystals of albite, b) Back Scattered Electron (BSE) image showing thin and bendable crystals of meta-autunite formed after dehydration process. The crystal are arranged to keep the approximate periphery of pre-existing autunite crystal.

Meta-autunite generally forms after autunite dehydration, where extremely fine fragments are formed by crystals fracturing. These fragments retain jointly the general form of autunite, and are therefore a pseudomorph of autunite. Meta-autunite appears as elongated crystals

with different sizes; they cluster in an array that makes it easy to draft an approximate periphery of the pre-existing autunite as shown in Figure 4b. Autunite crystals which exposed to the air for several months are at least partially transformed. Eventually, after many years, the meta-autunite might turn to fine particles or powder. Locock and Burns (2003) suggested that the rapid dehydration of autunite in air is associated with the underbonding at the Ca site and collapse of the structure. It is known that while the dehydration can be reversed and rehydrating back to autunite, the fragments do not combine back into a single crystal.

Uranyl Silicates

Uranyl silicates are the most abundant group of uranium minerals. This group is moderately soluble in water, so most uranyl complexes encountering free silicate ions might precipitate in the form of uranyl silicate. The XRD and EPMA data of the uranyl minerals from the study area showed the existence of uranyl silicate minerals represented mainly by uranophane, boltwoodite and soddyite.

Uranophane $Ca(UO_2)_2(SiO_3)_2\ (OH)_2.5H_2O$ occurs as lemon yellow to straw yellow radial aggregates in the voids and also as thin coatings along the fractures. The BSE images showed some uranophane crystals with matted intergrowth of minute fibers in a fan shape (Fig. 5a). Uranophane crystals are acicular and usually have a nearly square cross section (interfacial angle 97^o, Frondel, 1958). They show one perfect cleavage and traces from another parallel to crystal elongation. Uranophane is composed of sheets of uranyl cations $(UO_2)^{2+}$ coordinated by silicate tetrahedra. These sheets are stacked together to give a three dimensional matrix, and the charge is balanced in the structure by Ca^{2+} cations and water molecules that reside between the uranyl-silicate sheets (Ginderow, 1988). EPMA data of uranophane are given in Table 3. UO_3 ranges from 60.38 to 72.02 with an average of 67.52 %, SiO_2 ranges from 12.37 to 16.11 with an average of 14.33%, whereas CaO ranges from 2.33 to 7.19 with an average of 6.22%. Other minor constituents include Pb, Fe and P.

Boltwoodite $(H_3O)K[(UO_2)\ (SiO_4)].H_2O$ is a uranyl silicate of uranophane group mostly forms yellow radial aggregates or free acicular crystals (Fig. 5b). Table 3 shows the EPMA data of boltwoodite from the study area. UO_3 ranges from 59.05 to 70.66 with an average of 65.35%, SiO_2 ranges from 12.33 to 13.45 with an average of 12.78 %, K_2O ranges

from 2.56 to 8.54 with an average of 5.86%, whereas Na_2O ranges from 0 to 2.33% with an average of 0.84%.

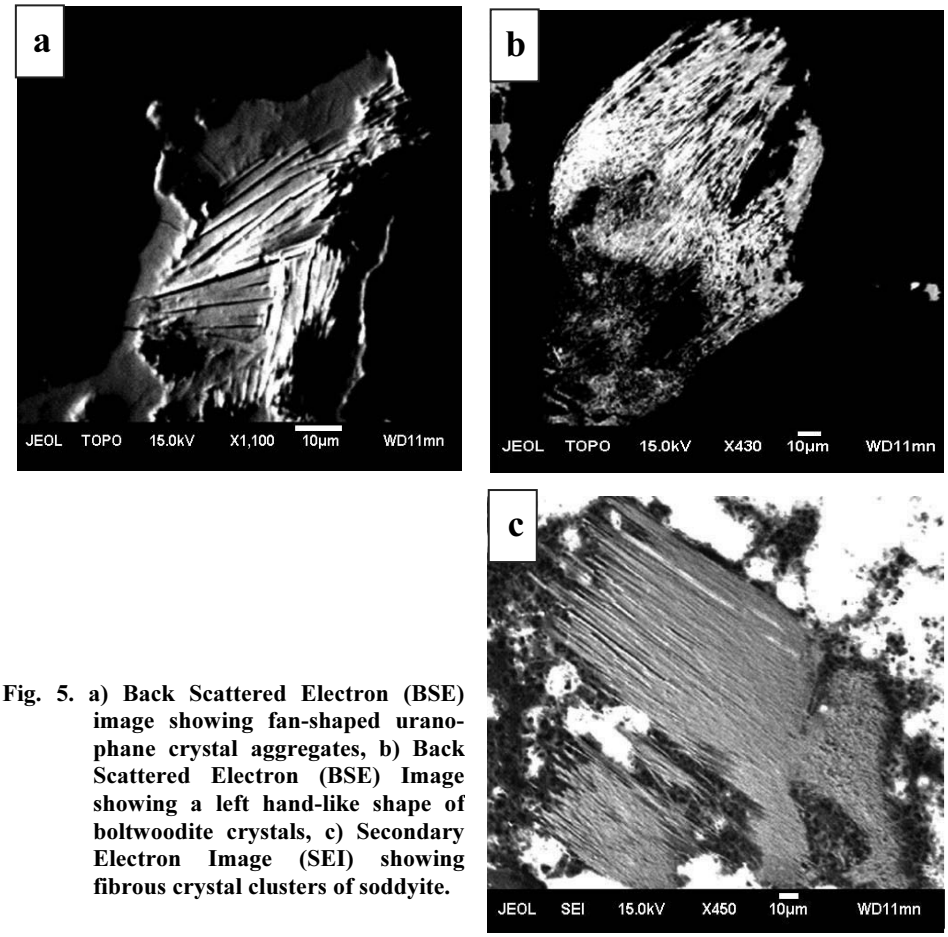

Fig. 5. a) Back Scattered Electron (BSE) image showing fan-shaped uranophane crystal aggregates, b) Back Scattered Electron (BSE) Image showing a left hand-like shape of boltwoodite crystals, c) Secondary Electron Image (SEI) showing fibrous crystal clusters of soddyite.

Soddyite $(UO_2)_2SiO_4(H_2O)_2$ occurs as orthorhombic pyramidal crystals. Its color ranges from greenish yellow to yellow. It occurs either as crystal clusters or as massive forms (Fig. 5c). Soddyite crystals are often distorted by elongation parallel to (110), giving a platy or prismatic appearance. Table 3 shows the EPMA data of soddyite from the study area. UO_3 ranges from 54.34 to 71.43 with an average of 66.45% whereas SiO_2 ranges from 10.93 to 15.35 with an average of 13.79%.

Table 2. Representative EMPA data (wt.%) of meta-autunite from Abu Rusheid area.

	Meta-autunite			
S.N.	1	2	3	4
SiO_2	1.08	1.13	0.41	1.33
P_2O_5	10.84	9.94	10.6	9.22
UO_3	76.27	74.98	72.43	68.54
CaO	1.57	1.86	1.86	1.15
Al_2O_3	0.71	0.01	0.06	0.14
V_2O_3	0.00	0.07	0.00	0.00
K_2O	0.06	0.27	0.03	0.00
Na_2O	0.00	0.11	0.01	0.00
MgO	0.03	0.01	0.02	0.02
Fe_2O_3	0.00	0.08	0.01	0.03
PbO	0.07	0.07	0.00	0.04
As_2O_5	0.00	0.00	0.08	0.03
La_2O_3	0.27	0.00	0.57	0.97
Ce_2O_3	0.20	0.01	0.19	0.63
Pr_2O_3	0.46	0.23	0.37	0.97
Nd_2O_3	0.00	0.02	0.00	0.11
Sm_2O_3	0.28	0.00	0.06	0.33
Eu_2O_3	0.04	0.07	0.16	0.05
Gd_2O_3	0.15	0.00	0.04	0.29
Tb_2O_3	0.11	0.00	0.00	0.16
Dy_2O_3	0.08	0.00	0.03	0.14
Ho_2O_3	0.26	0.00	0.17	0.25
Er_2O_3	0.00	0.00	0.07	0.00
Tm_2O_3	0.16	0.00	0.10	0.27
Yb_2O_3	0.17	0.00	0.06	0.00
Lu_2O_3	0.00	0.31	0.04	0.00
Total	92.81	89.16	87.37	84.65
a.p.f.u.		**based on 12 O**		
Si	0.168	0.185	0.069	0.231
P	1.420	1.380	1.490	1.360
U	2.480	2.570	2.530	2.500
Ca	0.261	0.326	0.330	0.214
Al	0.130	0.002	0.011	0.029
V	0.000	0.010	0.000	0.000
K	0.012	0.056	0.006	0.000
Na	0.000	0.035	0.004	0.000
Mg	0.007	0.002	0.002	0.005
Fe	0.000	0.010	0.010	0.004
Total	4.478	4.576	4.452	4.343

a.p.f.u. = atom per formula unit.
a.p.f.u. values of REE, As and Pb are very low and not represented here.

Table 3. Representative EMPA data (wt.%) of uranyl silicate minerals from Abu Rusheid area.

	Uranophane				Boltwoodite				Soddyite			
S.N.	5	6	7	8	9	10	11	12	13	14	15	16
SiO_2	13.11	13.00	15.92	13.24	12.33	12.74	13.45	12.77	10.93	15.35	13.39	12.89
P_2O_5	0.30	0.09	0.20	0.28	0.11	0.36	0.52	0.32	1.72	0.28	0.35	0.09
UO_3	64.21	67.31	66.95	66.44	59.05	61.45	62.96	58.25	54.34	71.43	65.76	62.98
CaO	6.15	6.55	6.34	6.78	0.12	0.01	0.15	0.06	0.87	0.55	0.46	0.09
Al_2O_3	0.03	0.03	0.61	0.03	0.00	0.00	0.18	0.02	0.00	0.04	0.08	0.06
V_2O_3	0.01	0.04	0.07	0.00	0.00	0.08	0.00	0.07	0.00	0.01	0.00	0.03
K_2O	0.00	0.00	0.00	0.00	7.45	7.81	5.45	8.54	0.00	0.00	0.00	0.00
Na_2O	0.00	0.01	0.14	0.20	0.21	0.06	2.33	0.00	0.00	0.00	0.00	0.00
MgO	0.00	0.00	0.03	0.03	0.00	0.00	0.02	0.00	0.04	0.05	0.01	0.00
Fe_2O_3	0.03	0.01	0.15	0.03	0.02	0.00	0.06	0.08	0.00	0.06	0.00	0.00
PbO	0.00	0.04	0.00	0.00	0.10	0.00	0.00	0.04	0.12	0.00	0.09	0.03
As_2O_5	0.00	0.09	0.00	0.01	0.00	0.00	0.00	0.01	0.08	0.05	0.00	0.00
La_2O_3	0.44	0.00	0.00	0.17	0.13	0.09	0.00	0.28	0.33	0.00	0.00	0.05
Ce_2O_3	0.21	0.00	0.00	0.02	0.17	0.04	0.06	0.00	0.17	0.02	0.06	0.09
Pr_2O_3	0.00	0.00	0.00	0.00	0.21	0.00	0.12	0.00	0.36	0.00	0.09	0.06
Nd_2O_3	0.00	0.08	0.00	0.04	0.00	0.09	0.02	0.00	0.07	0.00	0.00	0.00
Sm_2O_3	0.08	0.04	0.00	0.03	0.25	0.16	0.02	0.06	0.61	0.18	0.02	0.00
Eu_2O_3	0.11	0.00	0.00	0.03	0.00	0.00	0.00	0.00	0.10	0.00	0.00	0.00
Gd_2O_3	0.05	0.00	0.00	0.17	0.29	0.00	0.13	0.00	0.32	0.03	0.00	0.18
Tb_2O_3	0.00	0.00	0.20	0.00	0.14	0.00	0.00	0.00	0.00	0.00	0.10	0.32
Dy_2O_3	0.32	0.00	0.00	0.00	0.06	0.00	0.10	0.05	1.12	0.22	0.31	0.00
Ho_2O_3	0.00	0.00	0.00	0.01	0.07	0.19	0.00	0.00	0.06	0.12	0.00	0.00
Er_2O_3	0.00	0.20	0.06	0.00	0.00	0.09	0.09	0.00	0.53	0.03	0.00	0.06
Tm_2O_3	0.00	0.26	0.00	0.00	0.00	0.25	0.00	0.25	0.03	0.00	0.00	0.20
Yb_2O_3	0.00	0.00	0.01	0.12	0.00	0.00	0.00	0.10	0.88	0.03	0.06	0.02
Lu_2O_3	0.00	0.23	0.00	0.01	0.00	0.00	0.00	0.00	0.66	0.00	0.00	0.00
Total	85.05	87.98	90.68	87.64	80.71	83.43	85.67	80.90	73.34	88.46	80.78	77.16
a.p.f.u.	**based on 7 O**				**based on 7 O**				**based on 8 O**			
Si	1.229	1.194	1.344	1.206	1.269	1.264	1.268	1.295	1.377	1.584	1.531	1.552
P	0.021	0.007	0.014	0.021	0.012	0.035	0.047	0.023	0.180	0.020	0.030	0.010
U	1.267	1.295	1.190	1.267	1.272	1.283	1.248	1.237	1.440	1.550	1.580	1.590
Ca	0.618	0.644	0.573	0.662	0.013	0.001	0.015	0.007	0.117	0.061	0.056	0.012
Al	0.004	0.004	0.006	0.004	0.000	0.000	0.020	0.002	0.000	0.005	0.011	0.009
V	0.000	0.000	0.010	0.000	0.000	0.012	0.000	0.000	0.000	0.000	0.000	0.000
K	0.000	0.000	0.000	0.000	0.979	0.988	0.656	1.105	0.000	0.000	0.000	0.000
Na	0.000	0.002	0.023	0.035	0.042	0.012	0.426	0.000	0.000	0.000	0.000	0.000
Mg	0.000	0.000	0.003	0.004	0.000	0.000	0.002	0.000	0.008	0.008	0.002	0.000
Fe	0.002	0.001	0.010	0.002	0.001	0.000	0.005	0.006	0.000	0.005	0.000	0.000
Total	3.141	3.147	3.173	3.201	3.588	3.595	3.687	3.675	3.122	3.233	3.210	3.173

a.p.f.u. = atom per formula unit.

a.p.f.u. values of REE, As and Pb are very low and not represented here.

Discussions

The high-grade metamorphic rocks are consistently depleted in uranium relative to corresponding lower grade varieties suggesting that uranium can be mobilized and transported over significant distances during high-grade metamorphism (Skinner and Johnson, 1987). For example, uranium in mixed volcanic and sedimentary rocks in Bohemian massif has been mobilized during metamorphic, tectonic and igneous events and deposited in mylonitic and fault zones (Ruzicka, 1995). In the study area, since the primary uranium minerals as sources for uranyl phases in such metamorhphic environment are not recognized due to metamorphic processes, the later formed uranyl minerals were probably originated from U-rich arkose, greywacke and lithic arenite that formed in active continental margin and underwent metamorphism (Abd El-Naby and Frisch, 2006). Uranium originally occurred as disseminated or detrital minerals in the clastic sedimentary precursors. Hassan (1973) considered the U-rich thorite of the Abu Rusheid gneisses as a possible source for surficial uranyl mineralization. Metamict zircon and columbite could be also considered as additional sources for uranium (Finch and Murakami, 1999 and El-Kammar *et al.*, 2001). The possibility that uranium was introduced with younger granites in late stages or was related essentially to the older metasediments is abandoned for the low uranium contents of both rock types (average uranium contents of leucogranites is 1.5 ppm, Abd El-Naby and Frisch, 2006 and for metasediments is 2 ppm, Moghazi *et al.*, 2004).

When the radiogenic Pb accumulates in the structure of the uranium minerals, uranium content decreases concurrently (Fayek *et al.*, 1997). The analyses of uranyl minerals from the study area show low and variable PbO contents as well as a non-significant correlation between PbO and UO_3 (Fig. 6). This reflects that Pb does not exist as a radiogenic product and this could be regarded as an indication for young surficial uranyl mineralization. Similar uranyl mineralization associated with granitic and alkaline volcanic rocks in the Eastern Desert were reported as young deposits of a U-series age in the range of 50-159 ka (Osmond *et al.*, 1999 and Dawood, 2001). This correlation also indicates that Pb does not exist at the expense of uranium during a later phase of fluid/rock interaction and was probably carried by the same fluids that precipitated

uranyl minerals and not by post-mineralization fluid phases. Sources of Pb could be the sulphides associated with the studied gneisses.

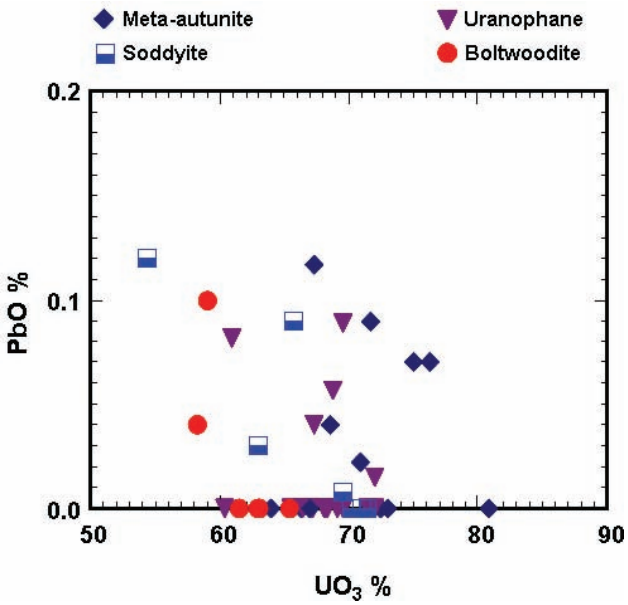

Fig. 6. Non-significant relationship between UO_3 and PbO of uranyl minerals. Samples with Pb contents are only used in this bivariant plot.

A few studies have revealed the presence of uranyl phosphate minerals together with uranyl silicates (Snelling, 1995 and Foord *et al.*, 1997). The present study showed the existence of meta-autunite in association with uranyl silicate phases represented by uranophane, boltwoodite and soddyite. The existence of these uranyl minerals along some parts of the shear zones in Abu Rusheid area could be interpreted by means of minerals paragenesis which can be recognized based on local groundwater chemistry.

Generally uranyl phosphates have solubility below those of uranyl silicates (Stumm and Morgan, 1981). They are usually formed by supergene alteration of U(IV) oxide minerals, U(VI)–Pb oxide minerals and U(VI) silicate minerals (Finch and Ewing, 1992; Isobe *et al.*, 1994; Murakami *et al.*, 1997; Sato *et al*., 1997 and Ragnarsdottir and Charlet, 2000). Uranyl phosphate minerals also occur by precipitation from groundwater (Dall'aglio *et al*., 1974). Gorman-Lewis *et al.* (2008) recognized uranyl phosphates as important phases for controlling

uranium mobility in the environment due to their extremely low solubility under circumneutral pH conditions. Isobe *et al.* (1995) have shown that U(VI) minerals containing P occur along the fractures of Fe-mineral veins at the oxidized zone of Oklo natural reactor. This also suggests that U(VI) mineralization occurs by other mechanisms than simple precipitation from groundwater. Precipitation of autunite on apatite surfaces was documented by Jerden and Sinha (2003) and Ohnuki *et al.* (2004). In the study area, autunite and meta-autunite were reported by Ibrahim *et al.* (2007) to be formed during hydrothermal activity.

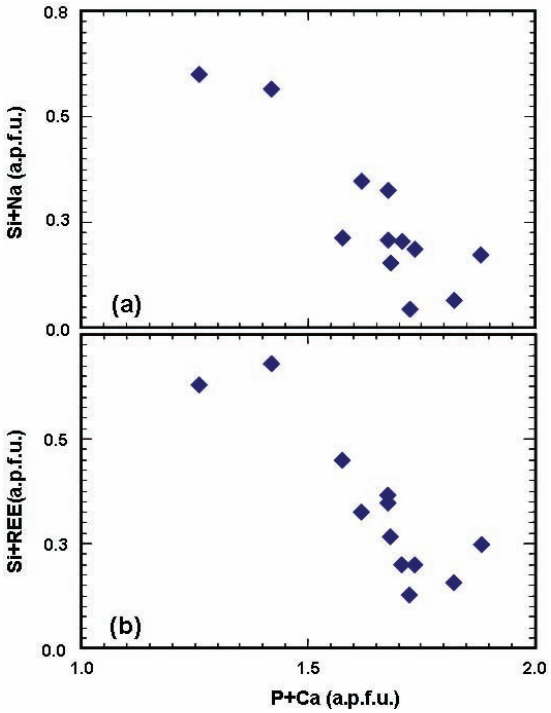

Fig 7. Bivariant plots reflecting substitutions of (P+Ca) by a. (Si+Na) and b. (Si +REE) in meta-autunite from the study area.

The structural formula of the uranyl minerals calculated from the microprobe data (Tables 2 and 3) deviates from their ideal compositions due to atomic substitution processes. The variation in chemical composition of meta-autunite is fairly in-herited from the pre-existing autunite. The coupled sub-stitutions of REE^{3+} or Na^{+} with Si^{4+} to replace P^{5+} and Ca^{2+} are confirmed from the bivariant relations (Fig. 7). The ionic radii of seven- and nine fold coordinated Na^{+} (1.12 and 1.24 Å, respectively) are close to those of Ca^{2+} (1.06 and 1.18 Å). So, the

replacement of Ca by Na is expected, but is controlled by charge-balancing mechanisms (Sha and Chappell, 1999). These kinds of substitutions were reported in phosphate minerals and could be summarized as follows:

$$3Na^{+} + Si^{4+} = P^{5+} + Ca^{2+}$$

$$REE^{3+} + Si^{4+} = P^{5+} + Ca^{2+} \qquad \text{(Roeder } et\ al.\text{, 1987)}$$

These substitutions may result in deficiency of P and Ca and enrichment of the other elements such as Si and REE in meta-autunite. Burns (1999) indicated that many uranyl phosphate minerals show substantial substitution of P. The substitution in autunite after precipitation was also reported by Simon *et al.* (2008) to modify the stoichiometric composition of the mineral. Stoichiometric uranium is also high in the meta-autunite analyses, which could be related to the substitution of $(UO_2)^{2+}$ for Ca^{2+}. This was confirmed by the experimental work of Ohnuki *et al.* (2004) where calcium decreases with increasing uranium during the autunite formation.

The association of uranyl minerals with a set of alteration products such as alunite, kaolinite, hematite and limonite suggests that the studied gneisses were affected by at least two phases of hydrothermal activities. The first phase started probably by the end of metamorphic process where hydrothermal fluids were formed mainly as a result of dehydration. Alternatively, this phase could have been started with the emplacement of younger granitic rocks. The chemistry of such fluids is strongly influenced by reactions with the host rock. These fluids were responsible for oxidation of sulphides and alteration of REE and U bearing minerals. P, Y and REE were released from the preexisting accessory phases such as monazite $(Ce,La,Y,Th)(PO_4)$ and apatite $Ca_5((F,Cl,OH)(PO_4)_3$. This is in accordance with the occurrence of surficial secondary yellow colored Y and REE enriched phases (Fig. 8). Supergene REE enrichment after weathering and alteration of the host rocks was also reported from other areas (Lewis *et al.*, 1998; Dawood *et al.*, 2004 and Liu and Zhang, 2005). Alteration of monazite during medium grade metamorphism from the eastern Alps was reported by Nagy *et al.* (2002). Papoulis *et al.* (2004) confirmed the alteration of monazite to a $ThSiO_4$ or Th–OH silicate in the gneissic weathering profiles of the Leucogia area. In the study area, ferrihydrite is formed

early during the alteration of ferrous minerals such as biotite and chlorite (Murakami *et al.*, 1996 and Krawczyk-Bärsch *et al.*, 2004). Dissolved P in circulating fluids probably was incorporated into ferrihydrite by adsorption, co-precipitation, or both (Murakami *et al.* 1997). Alunite was formed at this stage by the reaction of sulphuric acid with the orthoclase feldspar-rich parts of the rocks. Alunite deposits are known to be formed in the metamorphic rocks of a peraluminous parent rocks enriched in S and/or P (Dill, 2001).

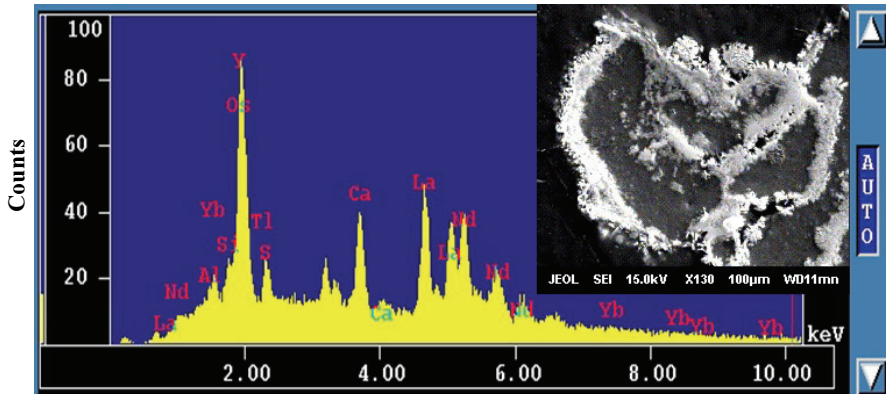

Fig. 8. SEI and EDX spectrum of a secondary unidentified Y, REE enriched mineral filling fractures and showing a fibrous habit.

A later phase of hydrothermal activity associated with quartz and pegmatitic veins started with more acidic affinity which is suitable for P releasing from ferrihydrite during its transformation to goethite and hematite (Murakami *et al.*, 1997) (Fig. 3). This P and locally available U combined in the presence of Ca to form autunite. Calcium availability is promoted by feldspars alteration. Figure 9 shows that the stability field of meta-autunite at 25 ^{o}C is in a pH range of 4.5-8.

$$Ca^{2+}_{(aq)} + 2(UO_2)^{2+}_{(aq)} + 2(PO_4)^{3-}_{(aq)} \rightarrow Ca(UO_2)_2(PO_4)_2.10–12H_2O_{(s)}$$

Autunite could also be formed locally at the expense of apatite in the shear zones. In this case, the formation of autunite occurs by local saturation rather than precipitation from bulk solution. This kind of replace-ment was reported within a similar oxidizing environment at the Sela shear zone in the south Eastern Desert of Egypt (Abd El-Naby and Dawood, 2008).

The residual fluids continued to move upwards through the pre-existing fractures and turned to be neutral to slightly alkaline which is a suitable medium for uranyl silicates precipitation (Fig. 9). The high specific surface area within the fractures facilitated the rapid dissolution of feldspars to replenish dissolved silica, causing saturation and precipitation of uranyl silicates. Studies of natural analogues and laboratory experiments indicate that uranyl silicates are likely to be the final uranyl mineral phases formed in the paragenetic alteration of spent nuclear fuel under oxidizing conditions when dissolved silica is present (Wronkiewicz *et al.*, 1996). The dispersion of uranyl silicates into the fractures was driven by the concentration gradient imposed by precipitation. The paragenetic sequence of uranyl minerals in the experiments reported by Wronkiewicz *et al.* (1992) is generally consistent with natural analogues. This sequence is uranyl oxide hydrates, soddyite, uranophane and boltwoodite. This paragenesis was reported in several deposits such as Nopal I deposit (Pearcy *et al.*, 1994). Occurrence of uranyl silicates suggested that they were favored at 1) alkaline pH, 2) abundant silica and 3) presence of void spaces. These three conditions were available in the study area during precipitation.

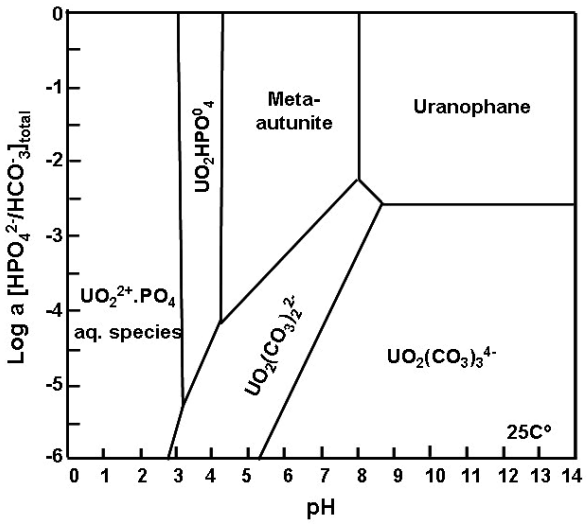

Fig. 9 Activity diagram showing U(VI) mineral stability of meta-autunite and uranophane as a function of the activity ratio of dissolved phosphate to carbonate *vs* pH, at 25°C. The diagram is modified after Jerden and Sinha (2003).

Most soluble uranium is transported in the oxidized, U (VI) oxidation state, bonded with oxygen to form uranyl ions (UO_2^{+2}). Uranyl carbonate, phosphate, sulphate and fluoride complexes greatly enhance the solubility of uranium (Langmuir, 1978). In the study area, carbonate complexes are of minor contribution since carbonate alteration such as secondary calcite is not present whereas uranyl sulphate complexes were probably more incorporated in uranium migration. The oxidation of sulphides by oxygen-bearing waters produces sulphate-rich acidic waters of pH < 5 (Brugger *et al.*, 2003). This water can leach and transport large quantities of uranium (Edwards *et al.*, 2000). Such waters are responsible for large-scale mobility of uranium and other actinides around uranium-bearing sites and tailing dumps, even long after mining has ceased (Fernandes *et al.*, 1995). Conversely, the association of uranyl silicates and fluorite in the fracture zones may reflect the role of fluoride complexes in the formation of uranyl silicates. The high mobility of fluorine in the study area during metasomatic processes was confirmed by Hassan (1973). The fluoride complexes in many uranium mineralizing systems are significant as indicated from the abundance of fluorite and other fluoride-bearing gangue minerals (Romberger, 1984). U^{+4}-fluoride complexes are stable below pH 4 providing a significant way of U migration in reducing groundwater (Parks and Pohl, 1988). Hydrothermal systems generally evolve from high temperature acid-reducing conditions to neutral oxidizing conditions (Eugster, 1984). Close to the surface, the oxygen fugacity (fO_2) increases and consequently, the uranous fluoride complexes, such as UF_4, would convert to uranyl fluoride complexes $UO_2F_3^-$ at slightly acidic to slightly alkaline medium. At the surface, the pressure decreases and the pH increases because of the loss of volatiles (Romberger, 1984). At these circumstances, the uranyl fluoride complexes become unstable and decompose in the presence of silicilic acid to form uranyl silicates and fluorite at low temperature conditions.

Uranophane precipitates from near neutral to alkaline groundwaters that contain Si and Ca (Korzeb *et al.*, 1997). The activities of Ca, K and Na control the respective stability of Ca- and K-Na uranyl silicates. Uranophane may crystallize for a range of Ca:Na or Ca:K ratios in solutions from 0.5:2 to 4:2; at low Ca-activity, boltwoodite is the stable phase (Cesbron *et al.*, 1992). The co-existence of both minerals in the study area reflects variation in the activity of these elements. This

variation depends on the composition of the dissolved minerals. The following reaction is suggested for the precipitation of uranophane from a fluid transported into fractures:

$2UO_2F_3^-{}_{(aq)} + 2(H_4SiO_4)_{(aq)} + 4Ca^{2+}{}_{(aq)} + 5H_2O \rightarrow Ca(UO_2)_2(SiO_3)_2(OH)_2.5H_2O_{(cr)} + 3CaF_{2(cr)} + 6H^+{}_{(aq)}$

Conversely, boltwoodite precipitated into fractures, where K is available, according to the following reaction:

$UO_2F_3^-{}_{(aq)} + K^+{}_{(aq)} + H_4SiO_{4(aq)} + 3OH^-{}_{(aq)} \rightarrow (H_3O)K[(UO_2)(SiO_4)].H_2O_{(cr)} + H_2O + 3F^-{}_{(g)}$

Sodium exists in the boltwoodite structure at the expense of K. The correlation coefficient between both elements in the boltwoodite from the study area is calculated as (-0.90). Several investigations have suggested that Na can partially replace K in the mineral structure (Stunz and Tennyson, 1983; Pu, 1990 and Burns, 1999). The structure of boltwoodite contains silicate tetrahedra and uranyl pentagonal bipyramids that share edges and corners to form alpha-uranophane type sheets (Burns, 1998). Such structure permits flexibility for cation substitution in the interlayer. Either K^+ or Na^+ can be accommodated in the interlayer between the sheets of silicate and uranyl polyhedra in the boltwoodite structure due to the presence of properly sized coordination polyhedra for both cations (Burns, 1998). This property improves the role of boltwoodite in determining the mobility of certain radionuclides in a geological repository. The K_2O-Na_2O-SiO_2 ternary diagram (Fig. 10a) confirms the presence of this kind of cation substitution in the boltwoodite from the study area. The occurrence of boltwoodite in fractures was reported in the deposit of the Delta Mine, Utah, where encrustations of boltwoodite were observed with other minerals immediately around oxidized uraninite, but boltwoodite was also observed as fine acicular crystals in rock fractures at some distance from the uraninite (Frondel and Ito, 1956). McKinley *et al.* (2006) concluded that the occurrence of boltwoodite in fractures reflects a migration of uranyl-rich solutions along a reacting flow path to a point where boltwoodite became supersaturated.

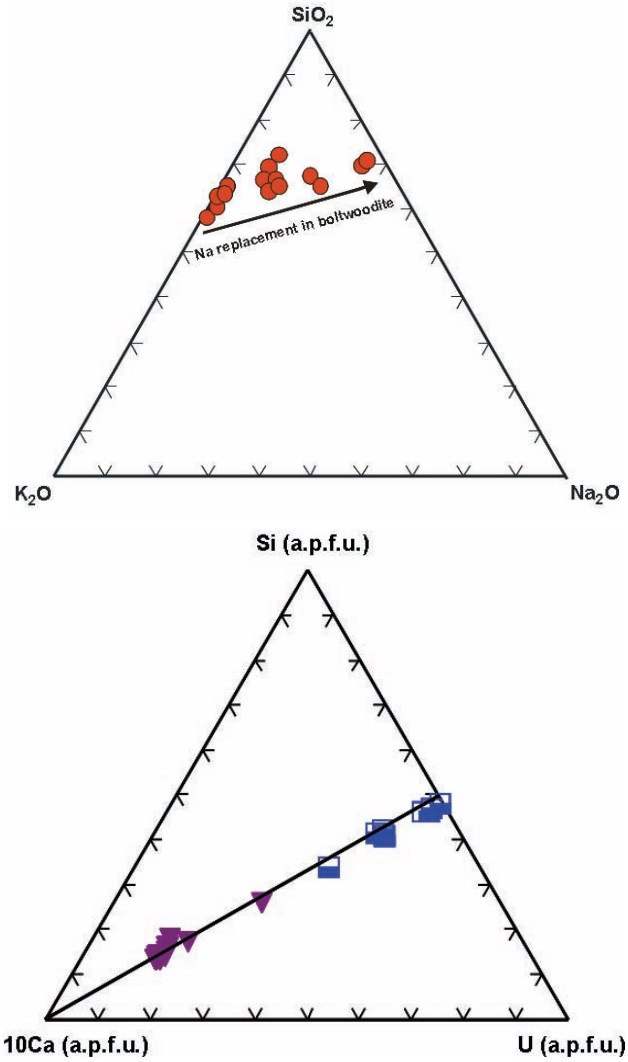

Fig. 10: a) K_2O-Na_2O-SiO_2 ternary diagram showing Na substitution for K in the boltwoodite from the study area, b) U-Ca-Si ternary diagram reflecting a genetic relationship between uranophane and soddyite. Symbols as in Fig. 6.

Soddyite could be formed by direct precipitation from the circulating fluids (Wronkiewicz *et al.*, 1992; Pearcy *et al.*, 1994 and Osmond *et al.*, 1999) or by replacement for uranophane (Finch, 1994). The replacement perception is probably more applicable in Abu Rusheid area as confirmed from the U-Ca-Si ternary diagram (Fig. 10b). The

uranophane and soddyite data are plotted along a single trend reflecting genetic relationship between the two minerals. Some uranophane crystals were later dissolved in dilute meteoric or groundwater at pH below than ~ 7, releasing Ca and silica to form soddyite (Deliens, 1977 and Finch, 1994). This kind of replacement was confirmed experimentally using deionized water (Cases *et al.*, 1994):

$$Ca(UO_2)_2(SiO_3)_2(OH)_2.5H_2O + 2H^+ \rightarrow (UO_2)_2SiO_4(H_2O)_2 + Ca^+ + H_4SiO_4 + 3H_2O$$

Uranophane Soddyite

Although the rainfall in the study area is scarce but local floods are reported to occur occasionally. This rainfall most likely provided the meteoric water required for such replacement. The precipitated uranyl silicates are currently immobile under the geochemical and hydrologic regime in the study area.

Conclusions

Uranium originally occurred in detrital minerals of the clastic sedimentary precursors of Abu Rusheid gneisses. Apparently the effect of metamorphism on the pre-existing uranium was limited to a more or less in situ remobilization and concentration of uranium without significant migration or removal as indicated by the common structural related mineralization. It is evident that Abu Rusheid gneisses have been exposed to a long period of alteration and rock–fluid interaction, providing the source for the formation of the uranyl minerals on the surface. The different alterations resulted from these solutions generally follow the main structural lines and shear zones. The rock–fluid interaction led to the breakdown of primary REE and Y-bearing minerals and release of REE as trivalent cations. The REE were incorporated later in secondary phases on the surface.

The paragenetic sequence of uranyl minerals in Abu Rusheid gneisses are autunite, uranophane, boltwoodite and soddyite (Fig. 11). The autunite has been extensively dehydrated later to meta-autunite. The meta-autunite fragments retain jointly the general form of autunite. The dispersion of uranyl minerals into the fractures was driven by the concentration gradient imposed by precipitation. Post mineralization fluids activity is confirmed based on the atomic substitutions in meta-autunite and soddyite replacement for uranophane. The mineral

chemistry and genesis of uranyl mineralization in the Abu Rusheid gneissic weathering profile are controlled by the radionuclides behavior in an arid environment and at extremely oxidizing conditions. These conditions are considered as analogous to those around radioactive waste repository in a similar rock type.

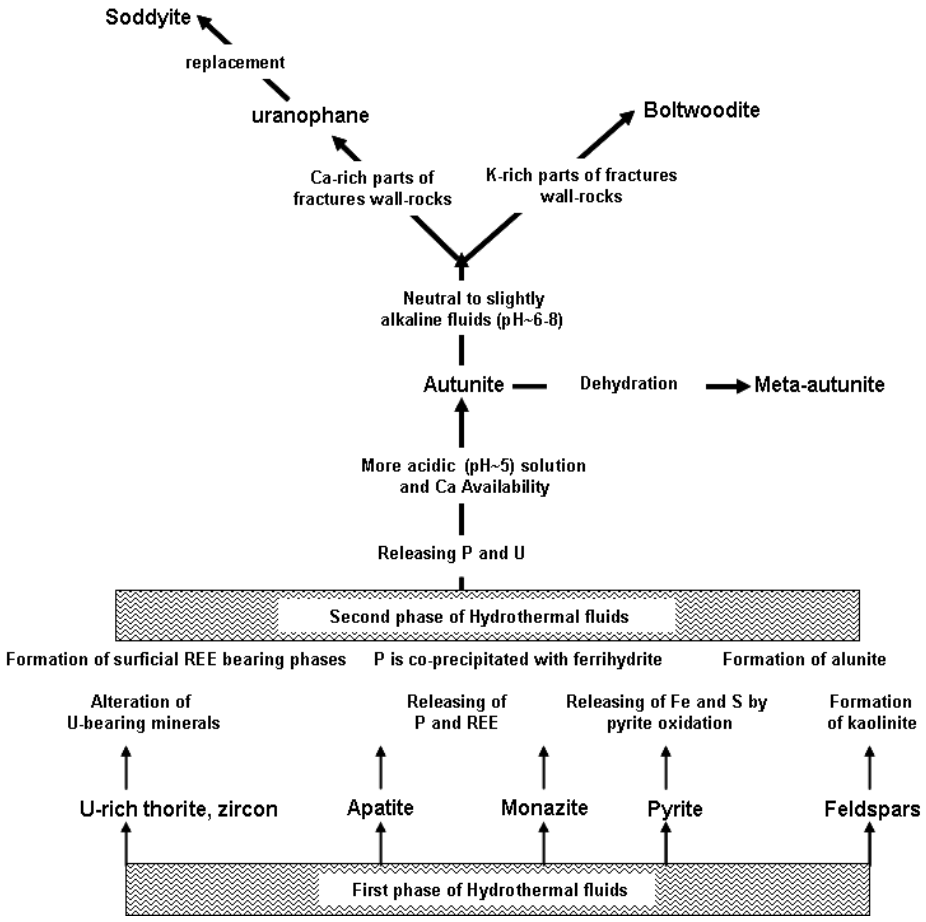

Fig. 11. Simplified paragenetic model of the uranyl minerals from the study area.

Acknowledgments

Thanks are due to the Institute of Geosciences, University of Tübingen, Germany for using their electron microprobe. H.H. Abd El-

Naby of the Egyptian Nuclear Materials Authority is gratefully acknowledged for various indispensable kinds of assistance.

References

Abd El-Naby, H.H. and **Dawood, Y.H.** (2008) Natural attenuation of uranium and formation of autunite at the expense of apatite within an oxidizing environment, south Eastern Desert of Egypt*, Applied Geochemistry,* **23:** 3741–3755.

Abd El-Naby, H.H. and **Frisch, W.** (2002) Origin of the Wadi Haimur–Abu Swayel Gneiss belt, South Eastern Desert, Egypt**:** Petrological and geochronological constraints, *Precambrian Research*, **113:** 307-322.

Abd El-Naby, H.H. and **Frisch, W.** (2006) Geochemical constraints from the Hafafit Metamorphic Complex (HMC): evidence of Neoproterozoic back-arc basin development in the central Eastern Desert of Egypt, *Journal of African Earth Sciences*, **45:** 173-186.

Abd El-Naby, H., Frisch, W. and **Siebel, W.** (2008) Tectono-metamorphic evolution of the Wadi Hafafit Culmination (central Eastern Desert, Egypt). Implication for Neoproterozoic core complex exhumation in NE Africa. *Geologica Acta*, **6** (4): 293-312.

Abdel-Monem, A.A. and **Hurley, P.M.** (1979) U-Pb staing of zircons from psammitic gneisses, Wadi Abu Rusheid-Wadi Sikait area, Egypt, *Institute of Applied Geology*, *Jeddah*, **3** (2): 165-170.

Brugger, J., Burns, P.C. and **Meisser, N.** (2003) Contribution to the mineralogy of acid drainage of uranium minerals: Marecottite and the zippeite-group, *American Mineralogist*, **88:** 676–685.

Burns, P.C. (1998) The structure of boltwoodite and implications of solid solution toward sodium boltwoodite, *The Canadian Mineralogist*, **36:** 1069-1075.

Burns, P.C. (1999) The crystal chemistry of uranium, In: P.C. Burns and R. Finch, (ed.), *Uranium: Mineralogy, Geochemistry, and the Environment,* Mineralogical Society of America, Washington, DC, **38:** 23–90.

Cases, I., Bruno, J., Cera, E., Finch, R.J. and **Ewing, R.C.** (1994) Kinetic and thermodynamic studies of uranium minerals. Assessment of the long-term evoultion of spent nuclear fuel. *SKB Technical Report 94-16*, Stockholm, 73.

Cesbron, F., Ildefonse, P. and **Sichere, M.C.** (1992) New mineralogical data on uranophane and beta-uranophane; synthesis of uranophane, *Mineralogical Magazine*: 301-308.

Dall'aglio, M., Gragnani, R. and **Locardi, E.** (1974) Geochemical factors controlling the formation of the secondary minerals of uranium. In: *Formation of Uranium Ore Deposits,* Inernational Atomic Energy Agency, Vienna, 33-48.

Dawood, Y.H., Abd El-Naby H.H. and **Sharafeldin A.A.** (2004) Influence of the alteration processes on the origin of uranium and europium anomalies in trachyte, central Eastern Desert, Egypt, *Geochemical Exploration*, **81:** 15-27.

Dawood, Y.H. (2001) Uranium-series disequilibrium dating of secondary uranium ore from south Eastern Desert of Egypt, *Applied Radiation and Isotopes*, **55** (6): 881-887.

Deliens, M. (1977) Associations de minéraux secondaires d'uranium à Shinkolobwe(région du Shaba, Zäire), *Bull. Soc. franç Minér. Crist.*, **100**: 32-38.

Dill, H.G. (2001) The geology of aluminum phosphates and sulphates of the alunite group minerals: A review, *Earth Science Reviews*, **53:** 35–93.

Edwards, K.J., Bond, P.L., Druschel, G.K., McGuire, M.M., Hamers, R.J. and **Banfield, J. F.** (2000) Geochemical and biological aspects of sulfide mineral dissolution: lessons from Iron Mountain, California, *Chemical Geology*: **169:** 383–397.

El Ramly, M. F., Greilling, R. O., Rashwan, A. A. and **Rasmy, A. H.** (1993) Explanatory note to accompany the geological and structural maps of Wadi Hafafit area, Eastern Desert of Egypt, *Geological Survey of Egypt*, Paper No. 68.

El Shazly, E. M. and **Hassan, M. A.** (1972) Geology and radioactive mineralization at Wadi Sikat-Wadi El- Gemal area, Eastern Desert, *Egyptian Journal of Geology*: **16:** 201-234.

El-Kammar, A. M., Salman, A. E., Shalaby, M. H. and **Mahdy A. I.** (2001) Geochemical and genetical constraints on rare metals mineralization at the central Eastern Desert of Egypt, *Geochemical Journal*, **35** (2): 117-135.

Eugster, H. P. (1984) Granites and hydrothermal ore deposits: a geochemical framework, *Mineralogical Magazine*, **49:** 7-23.

Ewing, R.C. (1991) The use of natural systems to predict radionuclide migration. Proceedings of the third international symposium on advanced nuclear energy research, global environment and nuclear energy, *Japanese Atomic Energy Research Institute*, 167.

Ewing, R.C. (1993) Long-term Predictions using Natural Analogous In: Murphy, W. M., Kovach, K. A. (ed.), The Role of Natural Analogs in Geologic Disposal of High-Level Nuclear Waste, *Proceedings of symposium sponsored by the Nuclear Regulatory Commission. Center for Nuclear Waste Regulatory Analyses,* Report 93-020, 29.

Fayek, M., Harrison, T.M., Ewing, R.C., Grove, M. and **Coath, C.D.** (2002) O and Pb isotopic analyses of uranium minerals by ion microprobe and U–Pb ages from the Cigar Lake deposit, *Chemical Geology*, **185:** 205-225.

Fayek, M., Janeczek, J. and **Ewing, R.C.** (1997) Mineral chemistry and oxygen isotopic analyses of uraninite, pitchblende and uranium alteration minerals from the Cigar Lake deposit, Saskatchewan, Canada, *Applied Geochemistry*, **12:** 549-565.

Fernandes, H.M., Veiga, L.H.S., Franklin, M.R., Prado, V.C.S. and **Taddei J.F.** (1995) Environmental Impact Assessment of Uranium Mining and Milling Facilities; a study case at the Pocos de Caldas uranium mining and milling site, Brazil. In: R.J. Allan and W. Salomons, (ed.), *Heavy Metal Aspects of Mining Pollution and its Remediation.* Elsevier, Amsterdam-New York, **52:** 161–173.

Finch, R. J. (1994) Paragenesis and crystal chemistry of the uranyl oxide hydrates, *Ph.D. Thesis,* University of New Mexico, 257 p.

Finch, R.J. and **Ewing, R.C.** (1992) The corrosion of uraninite under oxidizing conditions, *Journal of Nuclear Materials*, **190:** 133-156.

Finch, R. and **Murakami, T.** (1999) *Systematics and Paragenesis of Uranium Mineral.* In: P.C. Burns and R. Finch, (ed.), Uranium: Mineralogy, Geochemistry, and the Environment. Mineralogical Society of America, Washington, DC., **38**: 91–179.

Foord, E. E., Korzeb, S. L., Lichite, F. E. and **Fitzpatrick, J. J.** (1997) Additional studies on mixed uranyl oxide-hydroxide hydrate alteration products of uraninite from the Palermo and Ruggles granitic pegmatites, Grafton county, New Hampshire, *The Canadian Mineralogist*, **35:** 145-151.

Fowler, A. and **El Kalioubi, B.** (2002) The Migif-Hafafit gneissic complex of the Egyptian Eastern Desert: fold interference patterns involving multiply deformed sheath folds, *Tectonophysics*, **346:** 247-275.

Fowler, A. and **Osman, A. F.** (2009) The Shait-Nugrus shear zone separating central and south Eastern Deserts, Egypt: A post-arc collision low-angle normal ductile shear zone, *Journal of African Earth Sciences*, **53:** 16-32.

Frondel, C. (1958) Systematic mineralogy of uranium and thorium, *US Geological Survey Bulletin*, **1064**, US Government Printing Office, Washington, 400p.

Frondel, C. and **Ito, J.** (1956) Boltwoodite, a new uranium silicate, *Science*, **124:** 931.

Ginderow, D. (1988) Structure de l'uranophane alpha, $Ca(UO_2)_2[SiO_3(OH)]_2.5H_2O$, *Acta Crystallographica*, **C44:** 421-424.

Gorman-Lewis D., Mazeina, L., Fein, J.B., Szymanowski, J.E.S., Burns, P. C. and **Navrotsky A.** (2007) Thermodynamic properties of soddyite from solubility and calorimetry measurements, *Journal of Chemical Thermodynamics*, **39**: 568–575.

Gorman-Lewis, D., Burns, P.C. and **Fein, J. B.** (2008) Review of uranyl mineral solubility measurements. *Journal of Chemical Thermodynamics*, **40**: 335–352.

Greiling, R. O., Kröner, A., EI-Ramly, M. F. and **Rashwan. A. A.** (1988) Structural relationships between the southern and the central parts of the Eastern Desert of Egypt: details of a fold and thrust belt. In: S. EI-Gaby and R.O. Greiling, (ed.), *The Pan-African Belt of NE Africa and the Adjacent Areas.* Vieweg and Sohn, Wiesbaden, Germany: 121-146.

Harraz, H. Z., and **El-Sharkawy, M. F.** (2001) Origin of tourmaline in the metamorphosed Sikait pelitic belt, south Eastern Desert, Egypt, *Journal of African Earth Sciences*: **33** (2): 391-416.

Hassan, M. A. (1973) Geology and geochemistry of radioactive columbite-bearing psammitic gneiss of Wadi Abu Rusheid South Eastern Desert, Egypt, *Annals of the Geological Survey of Egypt*, **III**: 207-225.

Hilmy, M. E., El Bayoumi, R. M. and **Eid A. S.** (1990) Geology, geochemistry and mineralization of the psammitic gneiss of Wadi Abu-Rusheid, Eastern Desert, Egypt, *Journal of African Earth Sciences*, **2**: 197-205.

Ibrahim, M. E., El-Tokhi, M. M., Saleh, G. M., Hassan, M. A. and **Rashed, M. A.** (2007) Geochemistry of lamprophyres associated with uranium mineralization, Southeastern Desert, Egypt, *Chinese journal of geochemistry*, **26** (4), DOI: 10.1007/s11631-007-0356-4

Ibrahim, M. E., Assaf, H. S. and **Saleh, G. M.** (2000) Geochemical alteration and spectrometric analysis in Abu Rusheid altered uraniferous gneissose granites, south Eastern Desert, Egypt, *Chieme der Erde*, **60**: 173-188.

Isobe, H., Ewing, R. C. and **Murakami, T.** (1994) Formation of secondary uranium minerals in the Koongarra deposit, Australia: Unweathered zone, *Journal of Nuclear Materials*, **190**: 174-187.

Isobe, H., Ohnuki, T., Murakami, T. and **Gauthier-Lafaye, F.** (1995) Uranium redistribution under oxidation conditions in Oklo natural reactor zone 2, Gabon, *Proceeding of Material Research Soceity Symposium*, **353**: 1211–1218.

Janeczek, J., Ewing, R.C., Oversby, V.M. and **Werme, L.O.** (1996) Uraninite and UO2 in spent nuclear fuel: a comparison, *Journal of Nuclear Materials*, **238**: 121-130.

Jerden, J. L., Jr. and **Sinha A. K.** (2006) Geochemical coupling of uranium and phosphorous in soils overlying an unmined uranium deposit: Coles Hill, Virginia, *Journal of Geochemical Exploration*, 56–70

Jerden, J. L., Jr. and **Sinha A. K.** (2003) Phosphate based immobilization of uranium in an oxidizing bedrock aquifer, *Applied Geochemisty*, **18** (6): 823-843.

Korzeb, S.L., Foord, E.E., and **Lichte, F.E.** (1997) The chemical evolution and paragenesis of uranium minerals from the Ruggles and Palermo granitic pegmatites, New Hampshire, *Canadian Mineralogist*, **35**: 135–144.

Krawczyk-Bärsch, E., Arnold, T., Reuther, H., Brandt, F., Bosbach, D. and **Bernhard, G.** (2004) Formation of secondary Fe-oxyhydroxide phases during the dissolution of chlorite – effects on uranium sorption, *Applied Geochemistry*, **19**: 1403–1412

Langmuir, D. (1978) Uranium solution–minerals equilibria at low temperatures with applications to sedimentary ore deposits, *Geochimica et Cosmochimica Acta*, **42**: 547–569.

Lerouge, C., Kunov, A., Fléhoc, C., Georgieva, S., Hikov, A., Lescuyer, J. L., Petrunov, R. and **Velinova, N.** (2006) Constraints of stable isotopes on the origin of alunite from advanced argillic alteration systems in Bulgaria. *Journal of Geochemical Exploration*, **90**: 166–182.

Lewis, A. J., Komninou, A., Yardley, B. W. D. and **Palmer, M. R.** (1998) Rare earth element speciation in geothermal fluids from Yellowstone National Park, Wyoming, USA, *Geochimica. et Cosmochimica. Acta*, **62** (4): 657–663.

Liu, C. and **Zhang, H.** (2005) The lanthanide tetrad effect in apatite from the Altay No. 3 pegmatite, Xingjiang, China: an intrinsic feature of the pegmatite magma, *Chemical Geology*, **214**: 61–77.

Locock, A. J. and **Burns, P. C.** (2003) The crystal structure of synthetic autunite, Ca[(UO2)(PO4)]2(H2O)11, *American Mineralogist*, **88**: 240–244.

Loizenbauer, L., Wallbrecher, E., Fritz, H., Neumayr, P., Khudeir, A. A. and **Kloetzli, U.** (2001) Structural Geology, single zircon ages and fluid inclusion studies of the Meatiq metamorphic core complex: Implications for Neoproterozoic tectonics in the Eastern Desert of Egypt, *Precambrian Research*, **110:** 357–383.

Mansour, G. R. (2005) Geological and geophysical investigations of mineralized structures in Wadi Abalea and its surroundings, Abu Rusheid area, south Eastern Desert, Egypt, Unpublished *Ph.D. Thesis,* Mansoura University, Egypt, 139 p.

McKinley, J. P., Zachara, J. M., Liu, C., Heald, S.C., Prenitzer, B. I. and **Kempshall, B.W.** (2006) Microscale controls on the fate of contaminant uranium in the vadose zone, Hanford Site, Washington, *Geochimica et Cosmochimica Acta,* **70:** 1873–1887.

Moghazi, A.M., Hassanen, M.A., Mohamed, F.H. and **Ali, S.** (2004) Late Neoproterozoic strongly peraluminous leucogranites, south Eastern Desert, Egypt–petrogenesis and geodynamic significance, *Mineralogy and Petrology*, **81**, 19-41.

Murakami, T., Isobe, H., Sato, T. and **Ohnuki, T.** (1996) Weathering of chlorite in a quartz chlorite schist: I. Mineralogical and chemical changes, *Clays Clay Minerals*, **44:** 244-256.

Murakami, T., Ohnuki, T., Isobe, H. and **Sato, T.** (1997) Mobility of uranium during weathering. *American Mineralogist*, **82**: 888-899.

Nagy, G., Draganits, E., Demény, A., György, P. and **Árkai, P.** (2002) Genesis and transformations of monazite, florencite and rhabdophane during medium grade metamorphism: examples from the Sopron Hills, Eastern Alps, *Chemical Geology*, **191:** 25– 46.

Ohnuki, T., Kozai, N., Samadfam, M., Yasuda, R., Yamamoto, S., Narumi, K., Naramoto, H. and **Murakami, T.** (2004) The formation of autunite (Ca(UO2)2(PO4)2.nH2O) within the leached layer of dissolving apatite: incorporation mechanism of uranium by apatite, *Chemical Geology*, **211**: 1-14.

Osmond, J.K., Dabous, A.A. and **Dawood, Y.H.** (1999) U series age and origin of two secondary uranium deposits, central Eastern Desert, Egypt, *Economic Geology*, **94**: 273-280.

Papoulis, D. ,Tsolis-Katagas, P. and **Katagas, C.** (2004) Monazite alteration mechanisms and depletion measurements in kaolins, *Applied Clay Science*, **24**: 271– 285.

Parks, G.A. and **Pohl, D.C.** 1988. Hydrothermal solubility of uraninite, *Geochimica et Cosmochimica Acta*, **52:** 863-875.

Pearcy, E. C., Prikryl, J. D., Murphy, W. M. and **Leslie, B. W.** (1994) Alteration of uraninite from Nopal I deposit, Pena Blanca District, Chihuahua, Mexico, compared to degradation of spent nuclear fuel in the proposed U.S. high-level nuclear waste repository at Yucca Mountain, Nevada, *Applied Geochemistry*, **9**: 713-732.

Pu, C. (1990) Boltwoodite discovered for the first time in China, *Acta Mineralogica Sinica*, **10**: 151-160.

Ragnarsdottir, K.V. and **Charlet, L.** (2000) *Uranium Behaviour in Natural Environments,* In: J.D. Cotter-Howells, L.S. Cambellm, E. Valsami-Jones and M. Batchelder, (ed.), Environmental Mineralogy: Microbial Interactions, Anthropogenic Influences, Contaminated Land and Waste management. The Mineralogical Society of GB, Alden Press, Oxford.

Raslan, M. (2008) Occurrence of Ishikawaite (Uranium-Rich Samarskite) in the Mineralized Abu Rushied Gneiss, Southeastern Desert, Egypt, *International Geology Review*, **50** (12): 1132 – 1140.

Roeder, P.L., MacArthur, D., Ma, X.-P., Palmer, G.R. and **Mariano, A.N.** (1987) Cathodoluminescence and microprobe study of rare-earth elements in apatite, *American Mineralogist*, **72**: 801–811.

Romberger, S.B. (1984) Transportation and deposition of uranium in hydrothermal systems at temperatures up to 300°C: Geological implications, In: Vivo, B.D., Capaldi, F.I.G., Simpson, P.R. (ed.), *Uranium Geochemistry, Mineralogy, Geology, Exploration and Resources,* The Institution of Mining and Metallurgy, London: 12-17.

Roser, B.P. and **Korsch, R.J.** (1986) Determination of tectonic setting of sandstone-mudstone suite using SiO_2 content and K_2O/Na_2O ratio, *Journal of Geology,* **94**: 635–650.

Ruzicka, V. (1995) Vein uranium, In: O.R. Eckstrand, W.D. Sinclair and R.I. Thorpe, (ed.), *Geology of Canadian Mineral Deposit Types,* Geological Survey of Canada, Geology of Canada, **8**:277-285.

Sabet, A.H., Tsogoev, V.B., Bordonosov, V.P., Shablovsky, R.G. and **Kossa, M.** (1976) On the geologic structures, laws of localization and prospects of Abu Rusheid rare metal deposit. *Annals of Geological Survey of Egypt,* **VI**: 130-139.

Sato, T., Murakami, T., Yanase, N., Isobe, H., Payne, T.E. and **Airey, P. L.** (1997) Iron nodules scavenging uranium from groundwater, *Environmental Science Technology*, **31**: 2854-2858.

Sha, L.K. and **Chappell, B.W**. (1999) Apatite chemical composition, determined by electron microprobe and laser-ablation inductively coupled plasma mass spectrometry, as a probe into granite petrogenesis, *Geochimica et Cosmochimiva Acta*, **63**: 3861-3881.

Simon F. G., Biermann V. and **Peplinski B**. (2008) Uranium removal from groundwater using hydroxyapatite, *Applied geochemistry*, doi: 10.1016/j.apgeochem. 2008.04.025

Skinner, B. J. and **Johnson, C. A.** (1987) Evidence for movement of ore materials during high-grade metamorphism, *Ore Geology Review*, **2** (1-3): 191-204.

Snelling, A. (1995) The Failure of U-Th-Pb Dating at Koongarra, Australia, *Creation Ex Nihilo*, *Technical Journal*, **9** (1): 71-92.

Stumm, W. and **Morgan, J. J.** (1981) *Aquatic chemistry*, 2nd edition, Wiley-Interscience, New York, 780 p.

Stunz, H. and **Tennyson, C.** (1983) Boltwoodite aus S.W. Afrika, *Der Aufschluss*, **34**: 497-501.

Wronkiewicz, D. J., Bates, J. K., Gerding, T. J., Veleckis, E. and **Tani, B. S.** (1992) Uranium release and secondary phase formation during unsaturated testing of UO_2 at 90 ^oC, *Journal of Nuclear Materials*, **190**: 107-127.

Wronkiewicz, D. J., Bates, J. K., Wolf, S. F. and **Buck, E. C.** (1996) Ten-Year Results from unsaturated drip tests with UO_2 at 90° C: Implications for the geologic disposal of spent nuclear fuel, *Journal of Nuclear Materials*, **238**: 78-95.

كيميائية ونشأة معادن اليورانيل المصاحبة لصخور النيس البساميتى بمنطقة أبو روشيد بجنوب الصحراء الشرقية، مصر

يحيى حسن داود

كلية علوم الأرض، جامعة الملك عبد العزيز، ص.ب. ٨٠٢٠٦، جدة ٢١٥٨٩، المملكة العربية السعودية

المستخلص. وجدت معادن الميتاأوتونيت واليورانوفان والبولتووديت والصوديت كقشور صفراء اللون، وكبلورات إبرية في الفجوات، والشقوق، ونطاقات القص فى صخور النيس البساميتي بمنطقة أبو روشيد. تم استخدام الميكروسكوب المستقطب، وحيود الأشعة السينية، والتصوير بواسطة الإليكترونات المبعثرة للخلف، والتصوير بواسطة الإليكترونات الثانوية، والمسح بمطياف تشتت الطاقة، والتحليل الكمي بجهاز المسبار الإليكتروني، وذلك لقياس تركيب، وسلوك، ومصير العناصر الأساسية والشحيحة في بروفيل التجوية بصخور النيس. وقد تأكد وجود إحلالات مزدوجة في الميتاأتونيت، وإحلال الصوديوم محل البوتاسيوم في البولتووديت، وتكوين الصوديت على حساب اليورانوفان بمنطقة الدراسة. كان واضحًا أن تأثير عمليات التحول على اليورانيوم الأولى سابق التكوين كان محدودًا في الإذابة وإعادة التركيز في نفس المكان. نشأت معادن اليورانيل من الصخر المضيف بعد تعرضه لفترة طويلة من التغاير وتفاعل الصخور مع السوائل. حدث الفصل والتنوع في معادن اليورانيل نتيجة التباين التركيبي مابين السوائل المتنقلة، وتركيب الصخور محليًا في الكسور. يعكس تصاحب معادن سيليكات اليورانيل مع الفلوريت في نطق الكسر

دور مركبات الفلوريد في تكوين هذه المعـــادن. يمـــدنا كـــل مـــن التركيب ونشأة معـــادن اليورانيـــل المـــصاحبة لـــصخور النـــيس البيساميتى بمنطقة أبو روشيد بمعلومـــات إضـــافية عـــن ســـلوك العناصر المشعة في البيئة الجافة، وفي ظروف تأكسد قوية.